Nanoscale

Accepted Manuscript

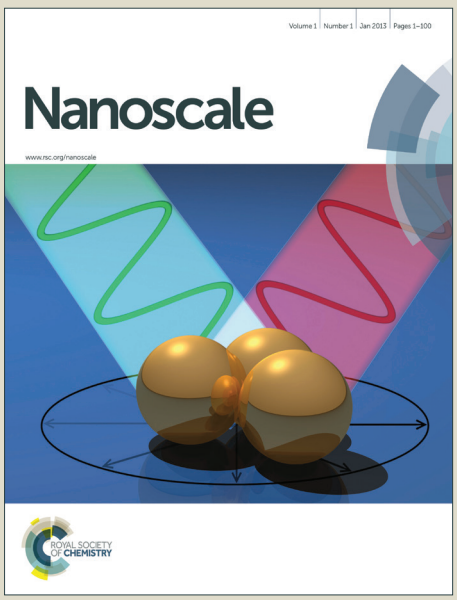

ROYAL SOCIETY OF CHEMISTRY

www.rsc.org/nanoscale

Cite this: DOI: 10.1039/c0xx00000x

www.rsc.org/xxxxxx

ARTICLE TYPE

Nuclear Uptake of Ultrasmall Gold-Doxorubicin Conjugates Imaged by Fluorescence Lifetime Imaging Microscopy (FLIM) and Electron Microscopy

Xuan Zhang [a], Sathvik Shastry [b], Stephen E. Bradforth [b], and Jay L. Nadeau*[a]

Received (in XXX, XXX) Xth XXXXXXXXX 20XX, Accepted Xth XXXXXXXXX 20XX

DOI: 10.1039/b000000x

Fluorescence lifetime imaging microscopy (FLIM) has been used to image free and encapsulated doxorubicin (Dox) uptake into cells, since interaction of Dox with DNA leads to a characteristic lifetime change. However, none of the reported Dox conjugates were able to enter cell nuclei. In this work, we use FLIM to show nuclear uptake of 2.7 nm mean diameter Au nanoparticles conjugated to Dox. The pattern of labelling differed substantially from what was seen with free Dox, with slower nuclear entry and stronger cytoplasmic labelling at all time points. As the cells died, the pattern of labelling changed further as intracellular structures disintegrated, consistent with association of Au-Dox to membranes. The patterns of Au distribution and intracellular structure changes were confirmed using electron microscopy, and indicate different mechanisms of cytotoxicity with stable Au-Dox conjugates compared to Dox alone. Such conjugates are promising tools for overcoming resistance in Dox-resistant cancers.

Introduction

Nano-gold is one of the most widely studied solid nanoparticles for use as a drug carrier. Several nanoparticle-gold preparations are currently in clinical trials; for a recent review, see [1]. Au nanoparticles are used for treating cancer by improving delivery of anti-cancer agents to tumors and/or by their own active properties, such as infrared absorption leading to local hyperthermia [2] [3] [4] or by amplifying the dose of therapeutic radiation [5], or a combination of both [6], which may be synergistic [7]. Despite a large body of literature, the ideal size and surface chemistry of gold nanoparticles for drug delivery has not been well established. Most studies have focused on 20-50 nm diameter particles with long circulation times (days). However, a recent study demonstrated specific gold accumulation in murine mammary tumors using 3.3 nm hydrodynamic diameter Au particles that were rapidly cleared by the kidney [8]. This suggests that inorganic solid nanoparticles for cancer imaging and therapy should be designed to permit renal clearance. This avoids the potential long-term risk of metals or semiconductors in the liver and spleen and facilitates regulatory approval [9] [10].

Ultra-small particles also have the advantage of being highly permeant to cells, including cell nuclei. In our previous work [11] we reported Au-tiopronin nanoparticles of mean diameter 2.7 nm, conjugated to doxorubicin (Dox) via an amide bond. These Au-Dox conjugates were taken up by B16 melanoma cells more efficiently than Dox alone and approximately 6-fold faster. The EC_{50} of Au-Dox was over 20-fold lower in B16 cells than that of Dox alone (17 μM for Dox alone vs. 930 nM with Au-Dox), but was slightly less than that of Dox alone in Dox-sensitive HeLa cells (1.5 μM for Dox alone vs. 2.5 μM for Au-Dox). Thus, Au nanoparticles appeared to reverse mechanisms of drug resistance found in B16 cells. Larger Au particles conjugated to Dox showed similar or reduced toxicity compared with Dox alone [12], with exclusion of Dox from the nucleus.

In this study we establish that the individual components of the conjugate—Dox and Au—enter the cell nuclei, using confocal imaging to image Dox fluorescence and atomic absorption spectroscopy (AAS) to quantify Au. However, these data do not establish that Au and Dox enter the nucleus together. Breakdown of the conjugates in cells due to lowered lysosomal pH, displacement of the Au surface thiols by glutathione, or other mechanisms might cause release of Dox from the particle surface with independent entry of the two components into the nucleus.

In order to determine whether Au-Dox entered the nucleus as a conjugate, we used fluorescence lifetime imaging microscopy (FLIM) to investigate cells at different time points during incubation with Dox and Au-Dox. Several previous studies have reported the use of FLIM to quantify uptake and release of encapsulated or conjugated Dox [13] [14] [15]. All of these report a longer lifetime of encapsulated Dox than of free Dox in either the cell cytoplasm or nucleus. There is some inconsistency in reported results of Dox lifetimes in cell nuclei, with one study reporting longer lifetimes than in cytoplasm [15], and two studies reporting shorter lifetimes [16] [13]. The long-lifetime component (~4.5 ns) is believed to represent Dox protected from water and oxygen, although this has not been fully investigated [15]. Another study investigated Dox bound to citric acid-γ-cyclodextrin and also reported a longer lifetime (2.4 ns), without an attempt to explain its origin [17]. In all previous work, encapsulated or conjugated Dox did not enter the cell nuclei. Conjugates were made with hydrolysable bonds to facilitate Dox release inside the cells, and release of Dox was seen as a shortening of fluorescence lifetime as the drug was liberated in the cytoplasm.

Our study is unique in two respects: first, in the use of a Dox conjugate with a stable bond which does not release Dox after 24 hours in situ incubation at pH 7 or pH 5; and second, in the use of an ultra-small nanoparticle which can cross the nuclear membrane. We chose this stable bond because of previous observations that the construct was highly effective against Dox-resistant cells, whereas it caused no additional toxicity in Dox-sensitive cells relative to Dox alone. The mechanisms of Au-Dox

cytotoxicity we observed were different from those of Dox alone; the former causes primarily caspase-independent cell death [11]. These results are consistent with previous studies using other types of stable conjugates, particularly Dox-transferrin, which has been investigated in great depth. Dox-transferrin conjugates do not require release for effectiveness, show greater activity against Dox-resistant cells than free Dox, and cause caspase-independent cell death [18-20]. The particle size was chosen because it permits nuclear uptake of both bare and Dox-conjugated particles. Although there is not a general consensus of the exact size and functionality of nanoparticle that will permit nuclear entry, particles of approximately the size used here have been seen to enter nuclei after 2 or more hours in several studies; particles of ~14 nm and larger are excluded [21-23].

Here we find that Au-Dox in bulk solution shows a dual-exponential lifetime that varies slightly as a function of concentration of Dox per particle. Changing pH, purging with N_2, or aggregating the particles does not substantially alter the lifetime, nor does incubation with genomic DNA. In all cases, the lifetime remains similar to that of free Dox. Previous studies have reported that liposomes do not affect Dox lifetime [24], but that cardiolipin, a component of mitochondrial and bacterial membranes, results in a lengthening of lifetime [25]. We thus incubated Au-Dox and Dox with spheroplasts or entire cells of *Escherichia coli*. A lengthened lifetime was observed consistent with that seen in mammalian cells.

In FLIM experiments using B16 melanoma cells, Au-Dox is visible as a long-lifetime component, similar to what is seen with Au-Dox in solution when exposed to membranes. The initial signal shows membrane-associated Au-Dox in the cytoplasm only, and unassociated or free Dox in the nucleus. Over the course of several hours, the Au-Dox conjugate enters the nucleus. The cells then begin to break down and release both cytoplasmic and nuclear components, with ultrastructural features suggesting a mix of apoptotic and necrotic processes. This study confirms the utility of ultra-small Au particles for drug delivery to cell nuclei, and suggests that the use of stable amide bonds permits efficient entry of Au-Dox into nuclei. It also suggests stronger and more complete association of Au-Dox with membranes than is seen with Dox alone, which may explain the different mechanisms of cell death observed with this conjugate.

Experimental section

Materials

All chemicals were purchased from Sigma-Aldrich and used without modification.

Particle synthesis and conjugation

The procedure for gold nanoparticle synthesis was adapted from the literature[26]. Hydrogen tetrachloroaureate(III) trihydrate (0.5 mmol) and tiopronin (N-(2-mercaptopropionyl)glycine) (1.2 mmol) were dissolved in 20 mL of methanol/acetic acid 6:1, and an aqueous solution of sodium borohydrate (7.5 mL, 8 mM) was slowly added. After vigorous stirring for 30 min, the resulting black solution was collected and concentrated. The residues were dissolved in 20 mL H_2O and dialyzed for 72 h against dH_2O (2 L), which was changed every 12 h. The resulting Au-tiopronin was lyophilized, weighed, and characterized by UV-Vis and fluorescence spectroscopy, Fourier transform infrared spectroscopy (FTIR), zeta potential, and transmission electron microscopy (TEM). Particle molecular weight was estimated using the mean diameter found by TEM in order to express particle concentration in M.

For conjugation to Dox, gold nanoparticles (100nM), 1-Ethyl-3-(3-dimethylaminopropyl)carbodiimide (EDC, 200μM) and N-hydroxysuccinimide (NHS, 400μM) were mixed in borate buffer (10mM, pH9) for 1h before doxorubicin (20 μM) was added. The reaction solution was stirred for 24h, filtered through a 3k M.W.C.O centrifugal filter (VWR) and cleaned 3 times with dH_2O. The concentration of unbound Dox was calculated from the absorbance of the filtrate at 480 nm using $\varepsilon = 11500$ L.mol^{-1}.cm^{-1}. Conjugates were stored at –20 ºC until ready for use.

To create particles with different levels of Dox conjugation, ratios of Au, Dox, EDC, and NHS were all varied: Au:Dox:EDC:NHS were 1:20:800:1600 for a "20 to 1" conjugate; 1:10:400:800 for a "10 to 1" conjugate; 1:5:200:800 for a "5 to 1" conjugate; and 1:1:40:80 for a "1 to 1" conjugate. Conjugates were cleaned by filtration and the amount bound quantified by UV-Vis.

Spheroplasts

Spheroplasts were prepared from stationary phase cultures of *Escherichia coli* strain AW405. The cells were pelleted, washed in phosphate-buffered saline (PBS), and then resuspended in 0.5 M sucrose in PBS. Lysozyme was added to a concentration of ~50 μg/mL and the cells were incubated at 37 º C for 2 h. A total of 10 mM EDTA was added in PBS, and the cells were returned to the incubator until spheroplast production was observed visually under a light microscope. When cells were ~ 80% spheroplasted, they were pelleted by centrifugation at 500 xg and washed with 0.25 M sucrose in PBS. One-half of this spheroplast mixture was added to 100 nM Au-Dox at 20: 1 or 2 μM Dox. 100 nM Au-Dox at 20: 1 was also added to a whole cell preparation of pelleted and washed E. coli at approximately the same cell density as the spheroplasts.

Doxorubicin release assay

The stability of the Dox nanoparticle conjugates was studied in acetate buffer at pH 5 or PBS at pH 7.4 and in the presence of glutathione (GSH). 400 μL of the conjugates were incubated with 5 μL of HCl (1 M) or GSH (2 mM) and shaken at 37 ºC for 0, 1, 2, 4, 5, 8, 10, and 24 h, then centrifuged through a centrifugal filter MWCO 3 KDa (VWR, modified PES 3K, 500 μL, low protein binding). The concentration of released Dox was measured from the absorbance at 480 nm in a plate reader (Molecular Devices M3).

Steady-state spectroscopy

Steady-state emission from Dox and Au-Dox was measured on a Fluoromax-3 fluorometer (Horiba Scientific) using an excitation wavelength of 500 nm. Bulk DNA was obtained from a genomic DNA preparation from *Escherichia coli* using a genomic DNA isolation kit (Qiagen).

Bulk TCSPC

Photoluminescence decays from bulk samples were obtained by the time-correlated single photon counting (TCSPC) technique. 800 nm laser pulses (~70 fs) out of a Coherent RegA 9050 Ti/sapphire regenerative amplifier operating at 250 kHz repetition rate were used to pump an OPA (Coherent 9450) which produced tunable visible light with an average power of ~30 mW. The beam was focused into the sample with a focal spot diameter of approximately 0.25 mm. The 500 nm excitation power delivered to the sample was set at 280 µW. The luminescence was collected with a 3.5 cm focal length lens placed perpendicular to the excitation beam and the collimated luminescence focused into a monochromator with a 10 cm focal length lens. The monochromator was a CVI CMSP112 double spectrograph with a 1/8 m total path length in negative dispersive mode with a pair of 600 groove/mm gratings (overall *f* number 3.9). The slit widths were 2.4 mm and based on a monochromator dispersion of 14 nm/mm, provided 10 nm resolution. A Hamamatsu RU3809 microchannel-plate photomultiplier was mounted on the monochromator exit slit. A Becker and Hickl SPC-630 photon counting board was used to record the time-resolved emission. The reference signal was provided by a portion of the excitation beam sent to a fast photodiode. To ensure good statistics, count rates were held at <1% of the laser repetition rate to avoid pulse pile up. Typical acquisition times were 10 minutes for a single scan. Lifetime decays of Dox were measured at 600 nm. The instrument response function (IRF) was determined from scatter off a solution of dilute coffee creamer. The full width at half-maximum of the IRF was 37 ps. Data analysis was performed using FluoFit 4.0 (PicoQuant, Berlin).

Cell culture and incubation

B16 melanoma cells were cultured in high-glucose DMEM (Invitrogen Canada, Burlington, ON) supplemented with streptomycin (100 µg/mL) and FBS (10%), and incubated in a 5% CO_2 humidified atmosphere.

AAS

B16 melanoma cells in 100 mm dishes at 80% confluency were incubated with Au-Dox or sham control (PBS) for 1 h or 4 h at a concentration of 5 nM Au nanoparticles. Incubation was performed in serum-containing DMEM. After incubation, cells were washed with PBS and trypsinized. Cell pellets were resuspended in digestion buffer (35% HCl and 7% HNO3 in H2O), sonicated for 5 min with a 25 kHz Ultrasonic Processor (SONOZAP), and incubated overnight at 70 °C. Both the cells and the nuclei were counted such that each sample contained same number of cells/nuclei before sonication. The final sample volume was adjusted to 1 mL with 0.2% HCl solution, and analyzed by atomic absorption spectroscopy (Perkin Elmer Analyst 800). To measure uptake into nuclei, cells immediately after trypsinization were run through with the nucleus isolation kit (Sigma-Aldrich NUC101). Nuclei were then treated for AAS as above. To calculate approximate concentrations in cells, cell volumes were estimated from images and flow cytometric data and compared with published results, with values of 20 µm cell diameter and 10 µm nuclear diameter used for the calculations.

Confocal imaging

B16 cells on glass-bottom dishes were incubated with Au-Dox at 1µM of Dox (40 nM of Au) for 1 h in Extreme DMEM (Wisent, Quebec, Canada), followed by washing twice with PBS and fixing with 2% of paraformaldehyde at 4 ºC for 10 min. Cells were then treated with DAPI (5 µg/mL) for 5 min, washed 3 times with ice-cold PBS and imaged in PBS. Laser-scanning confocal images were taken with a Zeiss LSM 510 meta confocor2 confocal microscope. Doxorubicin was excited with the 488 nm line of an Ar ion laser and DAPI was excited with a 405 nm blue diode laser.

Cell and nuclear volumes were estimated from confocal images of multiple cell fields using the automated cell counting features of ImageJ64.

FLIM

B16 cells on glass-bottom dishes were incubated with Au-Dox at 1µM of Dox (40 nM of Au) for 1h or with Au-Dox at 500 nM of Dox (20 nM of Au) for 2h, 4h, 12h, and 24h in Extreme DMEM (Wisent, Quebec, Canada). The concentration was reduced for longer incubations to minimize cell death. After incubation, cells were washed twice with PBS, fixed with 2% of paraformaldehyde at 4 ºC for 10 min, and washed 3 times with ice-cold PBS before imaging in PBS. Fluorescence lifetime images were acquired on a Zeiss LSM710 microscope outfitted with a PicoQuant LSM FLIM upgrade kit consisting of a FLIM excitation source, internal laser bypass, and single-photon avalanche diode (SPAD) detector. The excitation source was a 473 nm pulsed laser (PicoQuant LDH series) operated at a 50 MHz pulse rate (time resolution, 400 ps). Parameters were chosen so that unlabeled cell autofluorescence did not yield a measurable signal (zero counts). Signals were collected with a 590 nm long-pass filter for 90s with the pinhole open at 441.2 nm, and the gain set to 800. Data were analysed using SymPhoTme 64 (PicoQuant).

Lifetime decays from FLIM and bulk solution were fit to a multi-exponential decay model of the following form:

$$\frac{I}{I_0} = \sum_n a_n \exp\left(-\frac{t}{\tau_n}\right) \quad (1),$$

where a_n are the amplitudes and τ_n are the fluorescence lifetimes, with $n \leq 3$ for all cases. The instrument response function (IRF) was deconvolved from the signal. Goodness-of-fit data and residuals were used to gauge fit results; a χ^2 between 0.9-1.1 and random distribution of residuals around the x-axis were necessary for a fit to be considered accurate. Lifetime decay contributions were weighted by fractional intensity in reports of average FLIM lifetimes. Both amplitude- and intensity-weighted averages are given for bulk measurements.

Phasor analysis was performed using SimFCS (Laboratory for Fluorescence Dynamics, University of California, Irvine).

Electron microscopy

Cells for transmission electron microscopy were trypsinized, suspended in PBS, then fixed with 2.5 % (v/v) EM-grade glutaraldehyde. After 12-16 h fixation, cells were gently pelleted and washed in H_2O. The cells were dispersed into Noble agar worms, stained (or not) with 2 % OsO_4 and 2 % uranyl acetate

(UA), then dehydrated in ethanol and acetone before embedding in Eponate 12 resin. Sample resin blocks were trimmed and sectioned (50-60 nm) on a MT-X Ultramicrotome with a 45º Diatome diamond knife. Ultrathin sections were placed on 200 mesh formvar/carbon coated copper grids and imaged on a FEI XL 30 with a STEM detector at 30 kV and a working distance of 6.7 mm.

Results

Bulk emission and particle stability analysis

A TEM image of the Au nanoparticles is shown in **Fig. 1 A**. The particles had a zeta potential of -42 mV, which decreased to -28 mV upon Dox conjugation. They showed a weak near-IR emission (peak 780 nm, quantum yield < 0.1 %) but no absorbance plasmon peak (**Fig. 1 B**). Mean diameter as measured by TEM was 2.7 ± 0.9 nm, and with the typical conjugations conditions, were conjugated to approximately 25 Dox molecules per particle as measured by UV-Vis absorbance (for a schematic, see **Fig. 1 C**).

Conjugation of Au to Dox at a 1:25 ratio led to a significant quenching of Dox fluorescence intensity, >90% compared with Dox alone at equivalent Dox concentrations, but no shifts in the overall shape of the emission spectrum. The ratio of the peaks at 560 nm to that at 590 nm, which indicates dielectric environment [27], remained unchanged (**Fig. 2A**). Peak intensities were concentration-dependent in a nonlinear fashion, with self-quenching apparent at concentrations > 20 μM (**Fig. 2B**).

It has been shown that conjugation of ~5 fluorophores or more to a particle of this size will lead to dye-dye interactions [28], so conjugation of Au to different concentrations of Dox per particle, with subsequent purification, was also studied in order to investigate the mechanisms of Au-Dox interaction. These conjugates showed changes in both steady-state and time-resolved emission that varied somewhat with the amount of Dox conjugated. Both the emission of Dox and the near-IR Au nanoparticle fluorescence were reduced by conjugation (**Fig. 2 C**). The Stern-Volmer curve showed a plateau (not shown); a plot of reciprocal concentration vs. $I_0/(I_0-I)$ was linear, suggesting a sub-population of Dox that was accessible to the quencher [29] (**Fig. 2 D**).

Bulk TCSPC measurements of free doxorubicin yielded a lifetime of 1.0 ± 0.1 ns, consistent with literature results. This was independent of concentration across a wide range of samples tested (100 nM-1 mM) and did not change substantially when the sample was purged with N_2. Bulk lifetimes of Dox conjugated directly to Au particles have not previously been reported, although quenching of Dox by larger (plasmonic) particles has been used as a biosensor [30]. We found that Au-Dox showed a two-component decay consisting of a fast component that was either faster than that of free Dox (< 0.5 ns, for 1:1 conjugations) or comparable (1.1-1.2 ns, for all others), along with a substantially longer lifetime of 4-9 ns. The slower component was comparable to that seen previously with encapsulated Dox [13 15], but made up a very small contribution to the average lifetimes (**Fig. 3A**). When conjugation ratios were varied, lifetimes were essentially identical for all ratios except 1: 1 (**Fig. 3 B, Table 1**). Because the addition of unfragmented DNA to Dox has been shown to alter lifetimes, we also tested Dox and Au-Dox with bacterial genomic DNA at a ratio of 10:1 DNA: Dox. While a small change was seen in the lifetime of free Dox, there was no change in the lifetime of Au-Dox (**Table 1**). However, a striking effect was seen with the addition of bacterial spheroplasts. Both the lifetimes of Au-Dox and of Dox alone increased to 2.8 and 3.0 ns, respectively. However, the Dox alone signal was nearly 100-fold weaker than that of Au-Dox at the same concentration (**Fig. 3C, Table 1**).

Assays for released Dox indicated that the conjugates were stable over at least 24 h at both pH 7 (cytosolic) and pH 5 (endosomal), with statistically insignificant amounts of Dox release (data not shown).

Uptake of Dox, Au-Dox, and Au into cells by confocal and AAS

Confocal microscopy using native Dox fluorescence revealed striking differences in the pattern of uptake between free Dox and Au-Dox. Fluorescence from Au-Dox began to appear inside cells within 10 min, with peak signal occurring at approximately 1-2 h after conjugate addition. At later times, cells detached from the dish or were too fragmented to image (not shown). The signal was strongest in the nuclei, but significant fluorescence was also seen throughout the cytoplasm of most cells at the 2 h time point (**Fig. 4 A**). In contrast, the signal from free Dox was very weak until 50-60 min after drug addition, and remained strong for at least 24 h without signs of cell disintegration. Signal was almost exclusively nuclear (**Fig. 4 B**). The nuclei of Au-Dox cells were significantly smaller than those of Dox-only cells (150 ± 20 μm^2 for Au-Dox vs. 320 ± 30 μm^2 for Dox only, $n = 50$). The total cell volume was also reduced by approximately 50% as measured by flow cytometry for Au-Dox vs. Dox cells at the 2 h time point (not shown).

Atomic absorption spectroscopy (AAS) revealed that Au was present in cell nuclei isolated using molecular biology techniques. The time scale of nuclear Au incorporation was slower than that of the appearance of Dox-related fluorescence in the nucleus, with significant signal only after several hours of incubation (**Fig. 5**). This technique illustrated that Au could enter the nucleus, but did not prove that the Au particles were still attached to Dox at the time of entry. In addition, particles stuck to the nuclear membrane but not taken up into the nucleus would be included in the nuclear isolate. It was thus necessary to use FLIM and TEM to determine whether conjugated Au-Dox entered the nucleus.

We used the AAS data to estimate Au-Dox concentrations inside cells and nuclei. These values were largely in the tens of nM, assuming even distribution throughout the cell or nucleus (**Table 2**).

FLIM

Cells incubated with free Dox showed labelling primarily in the nucleus at time points of 1 h and longer. The decays of nuclear Dox fit to a single exponential with a lifetime of 1.3 ± 0.1 ns, (**Fig. 6A, C**). The cytoplasmic signal was weak but measurable, with a distinct peak at 2.6 ± 0.2 ns (see Supplementary Information **Fig. S1** for histograms from fits). These values were consistent with previous studies using free Dox. Incubation of cells with mixed but unconjugated Au nanoparticles and Dox led to a pattern identical to that of Dox alone (see Supplementary

Information **Fig. S2**).

At 1 hr, Au-Dox showed the strongest signal in the nucleus, with a weaker cytoplasmic signal with a longer lifetime (**Fig. 6 B, C**). Over the next several hours, cytoplasmic lifetimes continued to increase slightly, plateauing at a mean value near that of Au-Dox. The average lifetimes in the nucleus increased later, and reached levels intermediate between those of nuclear Dox and Au-Dox (**Fig. 6 D-I, Fig. 5 A**). At the 24 h time point, there was very little signal in the cell nuclei (**Fig. 6 H, I**).

Aggregates of Au-Dox that were not taken up into the cells were sometimes seen along the edges of the membrane; these exhibited a shorter lifetime than the Au-Dox inside cells (indicated by arrows in **Fig. 6 B, D**).

Pixel-by-pixel fits to the FLIM images showed double exponential decays at all time points, with two dominant lifetimes of ~1.3 ± 0.1 ns (corresponding to nuclear free Dox or free Au-Dox) and ~4.4 ± 0.1 ns (corresponding to membrane-bound Au-Dox) (**Fig. 7 B, Fig. 8**). At 1 hr, the Au-Dox sample showed a strong short-lifetime signal in the nucleus (**Fig. 8 A**). There was a very weak signal corresponding to free cytoplasmic Dox (2.6 ns) that appeared on the histogram, but which was dominated in the fits by the other components (see Supplementary Information **Fig. S1**). A signal from bound Au-Dox was apparent in the nucleus at 1 hr, and became stronger over the next 1-3 hr. The cytoplasmic Au-Dox signal also became stronger during this time (**Fig. 7 B, Fig. 8 B, C**). At 12 hr, there was almost no short-lifetime signal remaining in the nucleus, although a long-lifetime signal remained. However, there was a strong 1.3 ns signal throughout the cytoplasm at that time. The short-lifetime signal was diffuse, whereas the long-lifetime signal was associated with vesicles or blebs which could be clearly resolved in the intensity image (**Fig. 7B, Fig. 8 D**). At 24 hr, there was essential no nuclear signal, and the cytoplasmic signal corresponded to bound Au-Dox (**Fig. 7B, Fig. 8 E**). A phasor plot analysis is given in **Fig. 9**, showing lengthening of lifetimes with increasing incubation time.

While these images convincingly showed uptake of bound Au-Dox into cell nuclei, it did not explain the appearance of the short-lifetime component in cytoplasm at 12 h, or the disappearance of nuclear signal at 24 h. Possible explanations for the former include spillage of DNA-bound Dox out of the nucleus or release of Dox from Au-Dox in the cytoplasm, with lack of the usual lifetime lengthening because of destruction of cytoplasmic structures/organelles. Possible explanations for the signal at 24 h include expulsion of Dox from the nucleus or nuclear leakage/rupture. A series of transmission electron micrographs was taken to examine the cells during Au-Dox incubation.

TEM

Electron microscopy of Au-Dox labelled cells confirmed entry of Au particles into the nucleus after 1 hr of incubation (**Fig. 10 A, B**). At 6 hr, Au was present around the nuclear membrane as well as free in the nucleus; signs of organelle destruction were beginning to be apparent in the cytoplasm (**Fig. 10 C, D**). At 24 hr, mitochondria appeared swollen and destroyed, and the nucleus was shrunken and empty (**Fig. 10 E, F**).

Discussion and Conclusions

While several studies have reported bulk and cell-associated lifetimes of encapsulated Dox [13 15 14 31], this is the first to examine Dox bound via an amide bond to Au nanoparticles. The behaviour of the conjugates in bulk solution showed little change relative to Dox alone, despite strong steady-state quenching. This is consistent with at least two previous studies using fluorophores bound to ultra-small Au particles via short linkers, and may be due to static quenching, inner filter effects, or dye-dye interactions[32]. It is also not known why the Au fluorescence is reduced, though it is likely an inner filter effect. We did observe a reduction in lifetime at the lowest Dox:Au ratio tested (1:1), suggesting that in this case, dye-dye interactions may be significant. The Stern-Volmer plot suggested that some population of the Dox molecules were inaccessible to the quencher (i.e. the Au particle); this may represent "excess" Dox in the case of 25 Dox molecules per particle. We choose this concentration in order to maximize cytotoxicity and anti-tumor efficacy *in vivo*; however, clearer FLIM results might be obtained with lower concentration ratios, as it would enable a clear picture of whether some Dox is lost from the particle. The fraction of the decay that is fast changes with concentration, as seen in Fig. 3B, so it is possible that the two lifetimes represent different populations of Dox at different distances from the Au particle. Additional experiments with linkers of different lengths could help elucidate this observation. Future studies are underway in our group to quantify the photophysics of Au-Dox.

The bulk measurements help provide insight into what is observed in cells. When bacterial cells or spheroplasts are mixed with Dox and Au-Dox, lengthening of lifetimes occurs. However, the signal strength is nearly 100-fold greater for Au-Dox than for Dox alone at the same Dox concentration. This suggests that the Au-Dox associates much more strongly with membranes than free Dox, and/or that its emission is enhanced by this association. This corresponds well with what is seen in B16 cells, where a long lifetime consistent with membrane-associated Au-Dox dominates the signal in Au-Dox treated cells. In cells treated with free Dox, the signal was almost entirely nuclear, and the 3-4 ns lifetimes associated with membrane-bound Dox were not observed.

It is not entirely clear whether the shorter lifetimes seen in the nuclei reflect free Dox, non-membrane-associated Au-Dox, or some combination of both. Because free Dox and Au-Dox have similar lifetimes, quantitative measures of Au-Dox in the nucleus were not possible with FLIM. Nonetheless, the long-lifetime component could be readily used to observe uptake of Au-Dox into cells and nuclei. The appearance of the slow component in nuclei was consistent with the time course of gold entry seen with AAS and TEM. At 1 hr, most of the gold detected was in the cell cytoplasm; at 4 hr, a significant fraction was in the nucleus. The cytoplasmic labelling was diffuse, not endosomal as we have previously seen with quantum dots [33]. This is consistent with previous studies showing non-endosomal entry of ultra-small particles [34 35]; endosomal uptake also occurs, as seen in the TEM images. Endosomal uptake of such ultra-small particles has been shown to involve clusters of particles after they collect on the cell membrane [36].

At the earliest time point, some signal was seen that was likely

due to free Dox. This probably represented some small amount of free Dox that was not removed from the conjugates by dialysis and washing; it may also represent Dox displaced from the particles by cellular glutathione or non-membrane-associated Au-Dox. It was rapidly overwhelmed by the bound Au-Dox signal in the cytoplasm, and more slowly in the nucleus. Thus, if cellular processes are releasing Dox, this release appears to occur almost immediately after addition of the Au-Dox and not as a steady process.

Au-Dox labelled cells were characterized by reduced volume of the cytoplasm and the nucleus. By 12-24 h of incubation, the nucleus was reduced to a shrunken, empty membrane, with no fluorescent labelling apparent. Nuclear shrinkage is often associated with caspase-independent cell death. It is accompanied with the swelling of other organelles and vacuole formation. This is neither necrosis nor apoptosis, but the mechanism is not well understood [37]. TEM images also showed swollen mitochondria and destruction of other organelles at later time points. These features distinguish cell death due to Au-Dox from that due to free Dox, which is purely apoptotic.

Because Au-Dox lifetimes did not change with DNA addition, it was not clear from these experiments whether bound Au-Dox was still able to intercalate DNA. Nuclear damage due to Au-Dox might be due to different mechanisms than those usually attributed to free Dox. Previous studies have shown that Dox can bind to and damage membranes by both oxidative stress and direct binding to lipids; Dox-resistant cells show reduced lipid-bound Dox compared with sensitive cells [38]. In one study, transferrin-bound Dox was shown to be too large to enter cells efficiently, but nevertheless caused cytotoxicity almost equivalent to that of free Dox [18]. Transferrin-Dox was able to overcome Dox resistance in leukemia cells [19]. In another study, Dox stably conjugated to a polymer was shown to cause necrosis by membrane damage, without ever entering cell nuclei or inducing p53; the overall cytotoxicity of the polymer-bound Dox was lower than that of free Dox [39]. In the present work, Au-Dox may be damaging nuclear contents and membranes without intercalating into DNA. This would lead to substantial cell death by mechanisms different from those of Dox alone. However, we do observe some degree of apoptosis with Au-Dox. We thus suspect that this conjugate displays features of both bound and free Dox, which allows it to be more effective than Dox alone [11].

The enhanced entry of Au-Dox and these additional mechanisms of cytotoxicity may explain the ability of this conjugate to overcome Dox resistance. The use of stable conjugates of Dox to ultra-small nanoparticles is a promising approach to overcoming Dox resistance. It will be interesting for future studies to examine non-cancerous cells and cells that are highly sensitive to Dox, since it has been suggested that the association of Dox with membranes is different in resistant vs. sensitive cells[40-42].

Acknowledgement

XZ and JLN were funded by the CIHR Operating Grant MOP-133500, the NSERC Individual Discovery Program RGPIN 312970-2013, and the MDEIE PSR-SIIRI-562. JLN's salary support was provided by the Canada Research Chairs. We also thank Tse-Luen Wee for use and training of the FLIM instrument at McGill University, and Randall Mielke for assistance with the TEM. SS acknowledges USC Dornsife for a summer undergraduate research fellowship.

Notes and references

[a] *Department of Biomedical Engineering, McGill University, 3775 University Street, Montreal, QC H3A 2B4 Canada. Fax: 514 3987461; Tel: 514 3988372; E-mail: jay.nadeau@mcgill.ca* [b] *Department of Chemistry, University of Southern California, Los Angeles, CA 90089*

† Electronic Supplementary Information (ESI) available: Histograms of pixel-by-pixel fits; FLIM image of cells incubated with unconjugated Au and Dox; control TEM images. See DOI: 10.1039/b000000x/

References

1. Schutz, C. A., et al. *Nanomedicine (Lond)* **2013,** 8, (3), 449-67.
2. El-Sayed, I. H., et al. *Cancer Letters* **2006,** 239, (1), 129-135.
3. Gobin, A. M., et al. *Nano Letters* **2007,** 7, (7), 1929-1934.
4. Verma, J., et al., (1178-2013 (Electronic)).
5. Hainfeld, J. F., et al., (1361-6560 (Electronic)).
6. Huang, P., et al. *Biomaterials* **2011,** 32, (36), 9796-9809.
7. Kampinga, H. H., (0265-6736 (Print)).
8. Liu, J., et al. *J Am Chem Soc* **2013**.
9. Alric, C., et al. *Nanoscale* **2013,** 5, (13), 5930-9.
10. Zhang, X. D., et al. *International journal of nanomedicine* **2014,** 9, 2069-72.
11. Zhang, X., et al. *Bioconjug Chem* **2011,** 22, (2), 235-43.
12. Kumar, S. A., et al. *Nanotechnology* **2008,** 19.
13. Basuki, J. S., et al. *ACS Nano* **2013,** 7, (11), 10175-89.
14. Romero, G., et al. *Macromolecular bioscience* **2013,** 13, (2), 234-41.
15. Dai, X., et al. *Nanomedicine* **2008,** 4, (1), 49-56.
16. Chen, N. T., et al. *PLoS One* **2012,** 7, (9), e44947.
17. Anand, R., et al. *Photochemical & photobiological sciences : Official journal of the European Photochemistry Association and the European Society for Photobiology* **2013,** 12, (10), 1841-54.
18. Barabas, K., et al. *J Biol Chem* **1992,** 267, (13), 9437-42.
19. Lubgan, D., et al. *Cellular & molecular biology letters* **2009,** 14, (1), 113-27.
20. Szwed, M., et al. *Chemico-biological interactions* **2014,** 220C, 140-148.
21. Chithrani, B. D., et al. *Nano Lett* **2006,** 6, (4), 662-8.
22. Dykman, L. A.; Khlebtsov, N. G. *Chem Rev* **2014,** 114, (2), 1258-88.
23. Gu, Y. J., et al. *Toxicology and applied pharmacology* **2009,** 237, (2), 196-204.
24. Goldman, R., et al. *Biochimica et biophysica acta* **1978,** 512, (2), 254-69.
25. Malatesta, V.; Andreoni, A. *J Photochem Photobiol B* **1989,** 3, (2), 157-64.

26. Lopez-Cartes, C., et al. *J Phys Chem B* **2005,** 109, (18), 8761-6.

27. Karukstis, K. K., et al. *Biophysical chemistry* **1998,** 73, (3), 249-63.

28. Reineck, P., et al. *ACS Nano* **2013,** 7, (8), 6636-48.

29. Htun, T. *Journal of fluorescence* **2004,** 14, (2), 217-22.

30. Wang, F., et al. *ACS Nano* **2011,** 5, (5), 3679-92.

31. Duong, H. T., et al. *Molecular pharmaceutics* **2012,** 9, (11), 3046-61.

32. Carlini, L.; Nadeau, J. L. *Chemical communications* **2013,** 49, (17), 1714-6.

33. Wang, Y., et al. *ACS Nano* **2011,** 5, (12), 9718-25.

34. Lin, S. Y., et al. *Chemical communications* **2008**, (39), 4762-4.

35. Yang, L., et al. *Nanoscale* **2013,** 5, (4), 1537-43.

36. Shinzawa, K.; Tsujimoto, Y. *The Journal of cell biology* **2003,** 163, (6), 1219-30.

37. Awasthi, S., et al. *Cancer Lett* **1992,** 63, (2), 109-16.

38. Hovorka, O., et al. *Journal of controlled release : official journal of the Controlled Release Society* **2002,** 80, (1-3), 101-17.

Cite this: DOI: 10.1039/c0xx00000x

www.rsc.org/xxxxxx

ARTICLE TYPE

Table 1. TCSPC fit parameters for Dox and Au-Dox in solution under different conditions. A_1 and A_2 represent amplitudes of each component.

Sample	A_1	τ_1 (ns)	A_2	τ_2 (ns)	<τ> (ns) (amplitude weighted)	<τ> (ns) (intensity weighted)
Dox alone	34343	1.0	--	--	1.0	1.0
Dox alone N_2	929	1.1	--	--	1.1	1.1
Dox + DNA	5303	1.0	--	--	1.0	1.0
Dox alone spheroplast	217	1.00	223	3.56	3.0	2.3
Au-Dox 1:1	746	0.39	372	1.34	1.0	0.7
Au-Dox 5:1	2250	1.02	21.9	4.70	1.2	1.1
Au-Dox 10:1	4033	1.10	15.0	5.57	1.2	1.1
Au-Dox 20:1	7781	1.12	4.48	9.72	1.2	1.1
Au-Dox 25:1	15168	1.11	93.1	5.29	1.2	1.1
Au-Dox pH 5	9167	1.12	1.50	14.2	1.2	1.1
Au-Dox pH 4, aggregated	1632	1.14	19.0	4.81	1.3	1.2
Au-Dox N_2	11322	1.12	12.4	5.89	1.3	1.2
Au-Dox spheroplast	21171	1.37	10543	3.87	2.8	2.2
Au-Dox *E. coli*	22.0	1.33	16.9	4.71	3.8	2.8
Au-Dox +DNA	52322	1.09	309	4.25	1.2	1.1

Location	# of particles	Concentration
Cells (1h)	23900±300	~10 nM
Cells (4h)	63200±200	~30 nM
Nuclei (1h)	8000±500	~30 nM
Nuclei (4h)	43400±300	~170 nM

Table 2. Concentration of Au nanoparticles in regions measured by AAS at different times. Values are means of 3 independent experiments ± SD.

Cite this: DOI: 10.1039/c0xx00000x

www.rsc.org/xxxxxx

ARTICLE TYPE

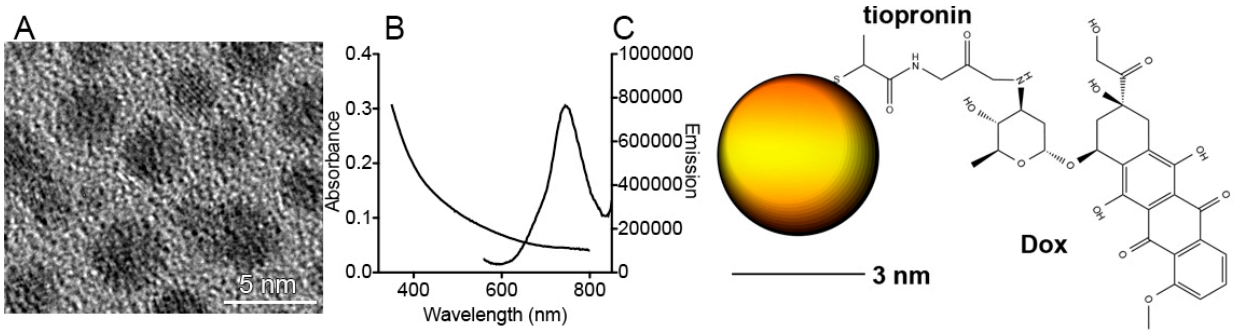

Figure 1. Au nanoparticles and conjugates. (A) TEM image of tiopronin-capped Au nanoparticles. (B) Absorbance and emission spectra (arbitrary units) of 1 μM Au nanoparticles. (C) Schematic of conjugation of Dox to the carboxylate group of tioponin, creating an amide bond.

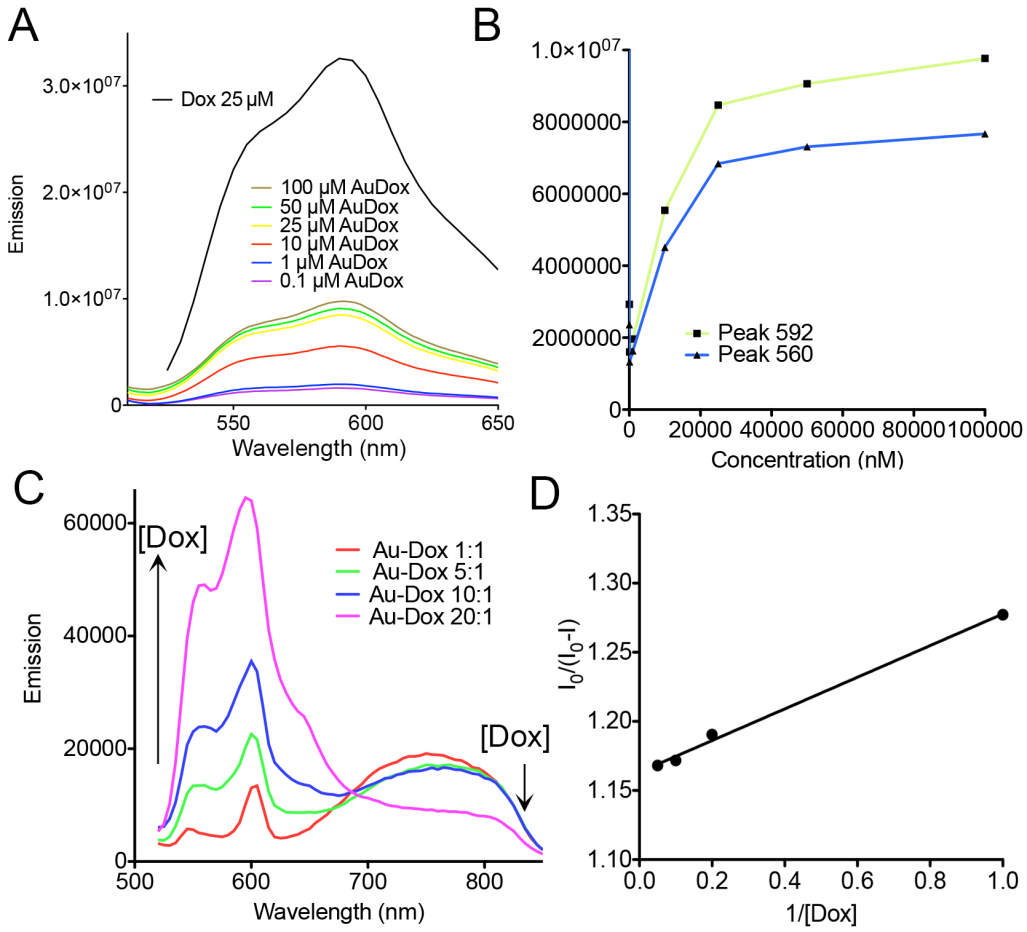

Figure 2. Steady-state emission properties of Au-Dox. (A) Conjugates at 25: 1 Dox: Au at different concentrations of Au (emission of 25 µM Dox shown for reference). (B) Emission peaks at 560 nm and 592 nm with concentration. (C) Conjugates made with different ratios of Dox: Au, showing emission spectra into the near-IR. Concentration of all samples is 100 nM Au. The emission of the Au particles decreases with increasing Dox coverage. (D) Non-linear Stern-Volmer plot for quenching of Au-Dox conjugates relative to Dox alone.

.

Cite this: DOI: 10.1039/c0xx00000x

www.rsc.org/xxxxxx

ARTICLE TYPE

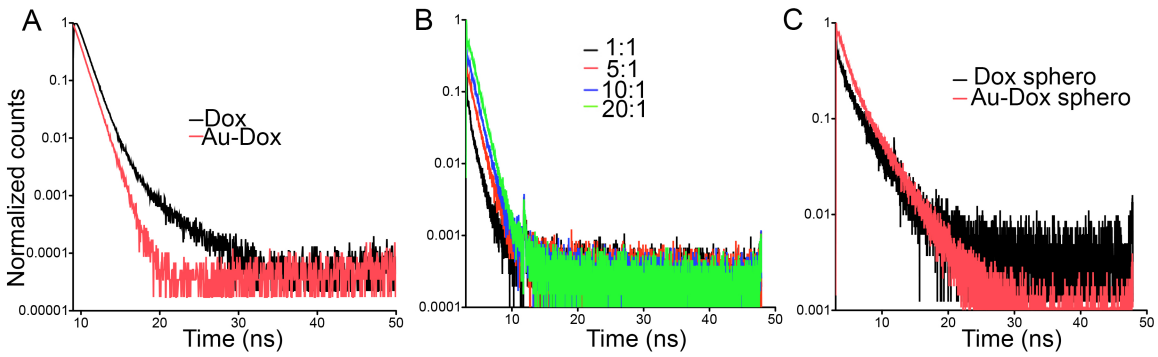

Figure 3. Lifetime decays of Dox and Au-Dox under different conditions. (A) Au-Dox vs. Dox alone at 100 nM, showing a small contribution of a longer lifetime in Au-Dox. (B) Au-Dox conjugated at different ratios (the time axis is somewhat compressed relative to panel A). (C) Dox and Au-Dox exposed to *E. coli* spheroplasts.

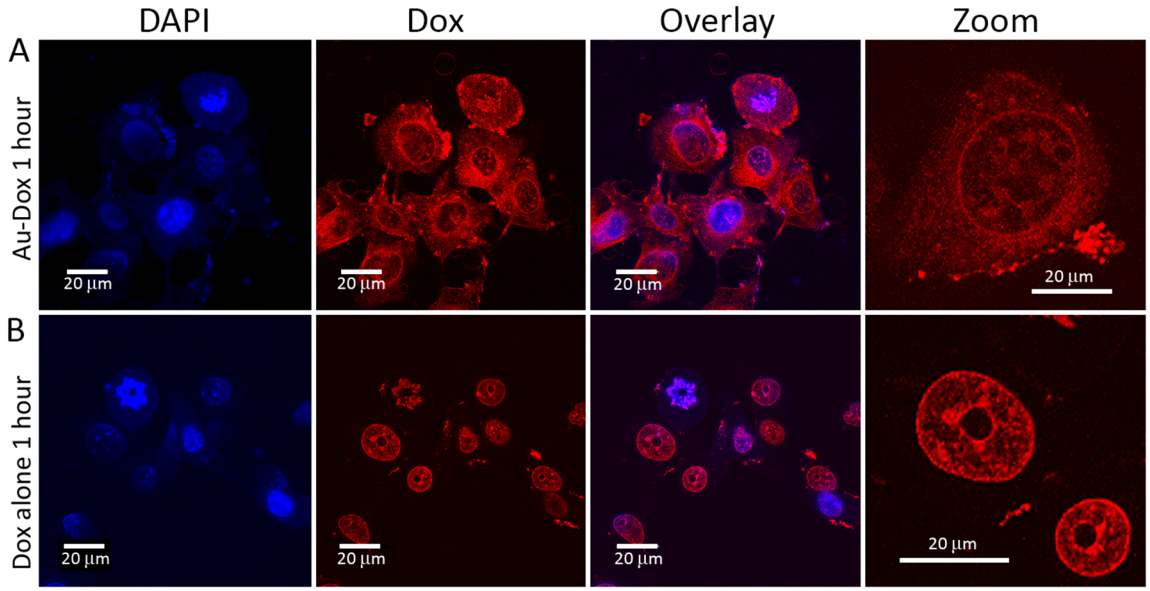

Figure 4. Uptake pattern of Au-Dox vs. Dox alone under confocal microscopy (excitation 488 nm, emission 590 ± 40). (A) Fluorescence images of Au-Dox in B16 cells after 1 h incubation showing intense nuclear labeling and significant cytoplasmic labeling. DAPI is included to show nuclei. (B) Fluorescence image of free Dox in cells after 1 h incubation showing staining restricted to the nucleus. Note that DAPI staining in dead cells is brighter than in live cells.

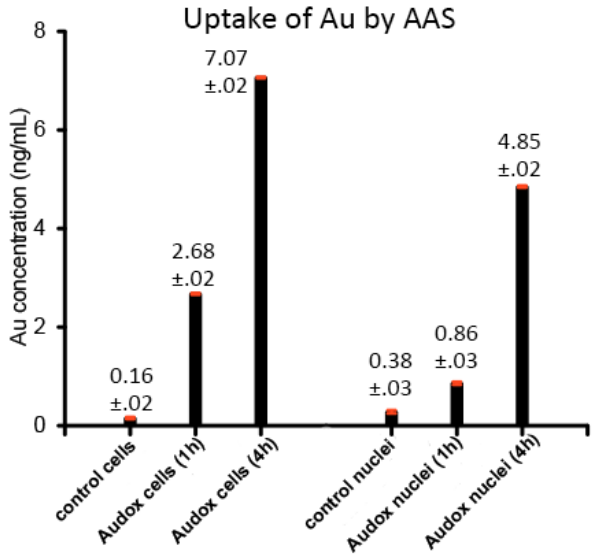

Figure 5. Au concentration in whole cells and isolated nuclei for cells incubated with Au-Dox for 1 h and 4 h.

Cite this: DOI: 10.1039/c0xx00000x

www.rsc.org/xxxxxx

ARTICLE TYPE

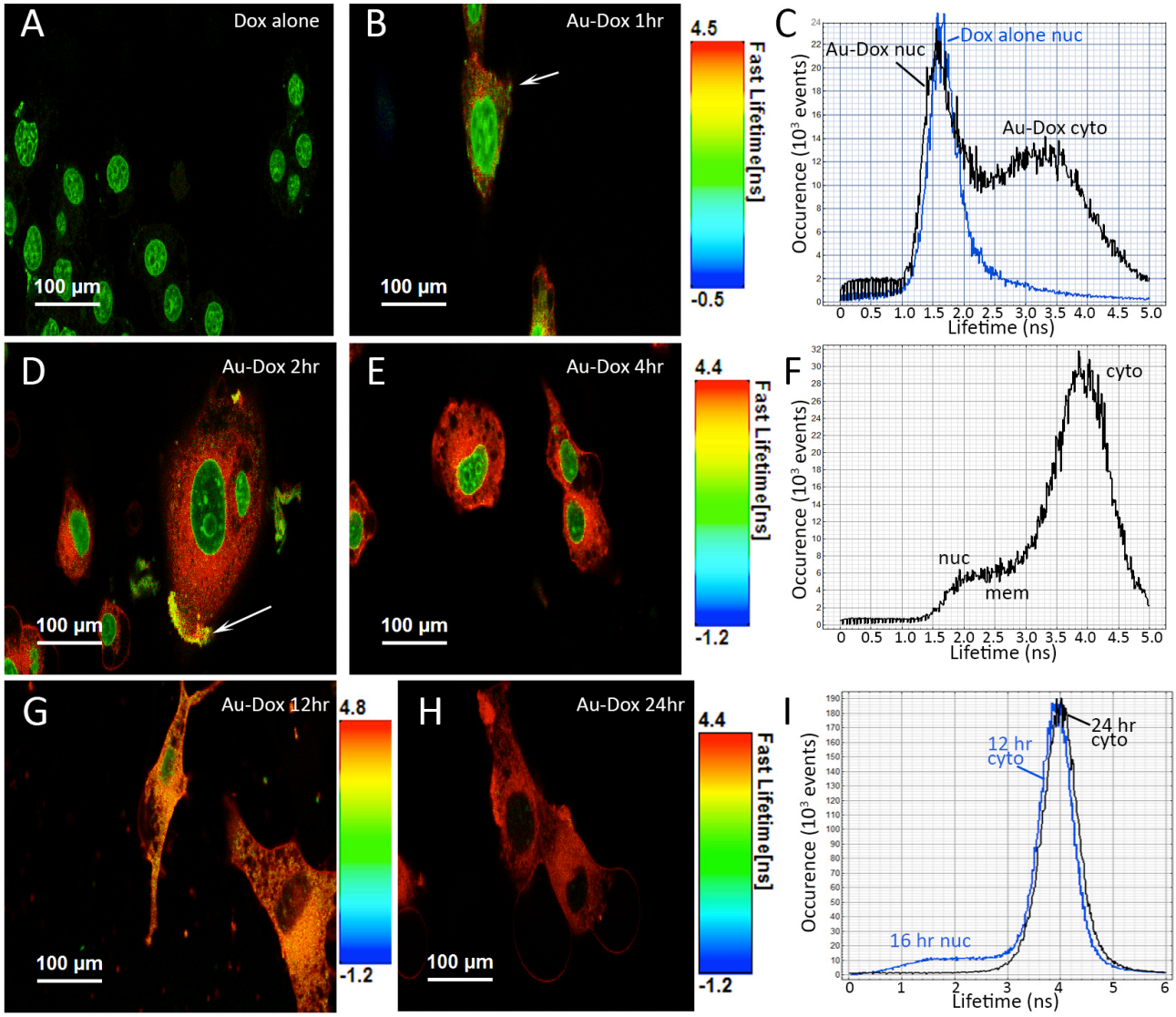

Figure 6. FLIM images and histograms of B16 cells incubated with free Dox for 1 hr or with Au-Dox for varying periods of time. (A) Free Dox collects in the nucleus within 1 hr; a weak cytoplasmic signal is seen with a lifetime of ~3 ns, but the signal is dominated by the 1.3 ns nuclear decay. (B) Au-Dox for 1 hr shows a strong nuclear signal identical to that of free Dox, with weaker cytoplasmic labeling. The arrow indicates an area of decreased lifetime on the edge of a cell suspected to be due to concentration effects. (C) Histograms for Dox alone vs. Au-Dox at 1 hr. (D-F) At 2 hr and 4 hr, Au-Dox shows a strong cytoplasmic signal and a weaker nuclear signal. The arrow indicates an aggregate showing a reduced lifetime, probably due to failure to associate with cells. Histograms are similar at both time points; Panel F shows the histogram for the 2 hr sample. (G-I) With increasing time of incubation, the short-lifetime nuclear signal gradually disappears while the long-lifetime cytoplasmic signal strengthens.

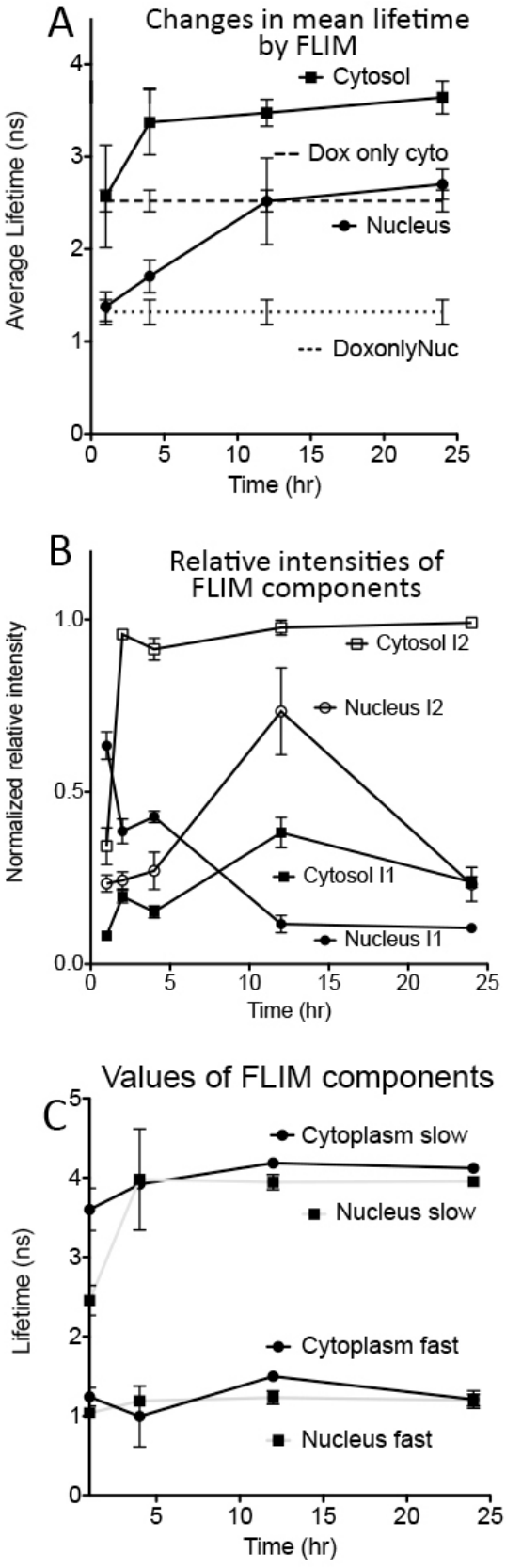

Figure 7. FLIM parameters from images in Figures 4 and 6. Error bars are means of 5-10 measurements with standard deviations shown; when error bars do not appear, they are smaller than symbols (A) Mean lifetimes measured at 10 discrete spots within the cytosol or nucleus at different time points of incubation with Au-Dox (error bars are standard deviations). The free Dox values were constant with time and are indicated by straight dashed lines. (B) Normalized relative intensities of the fast component (~ 1.3 ns, I1) and slow component (~4.4 ns, I2) in the nucleus and cytosol of selected cells. (C) Values of the fast and slow components in the cytoplasm and nucleus.

Cite this: DOI: 10.1039/c0xx00000x

www.rsc.org/xxxxxx

ARTICLE TYPE

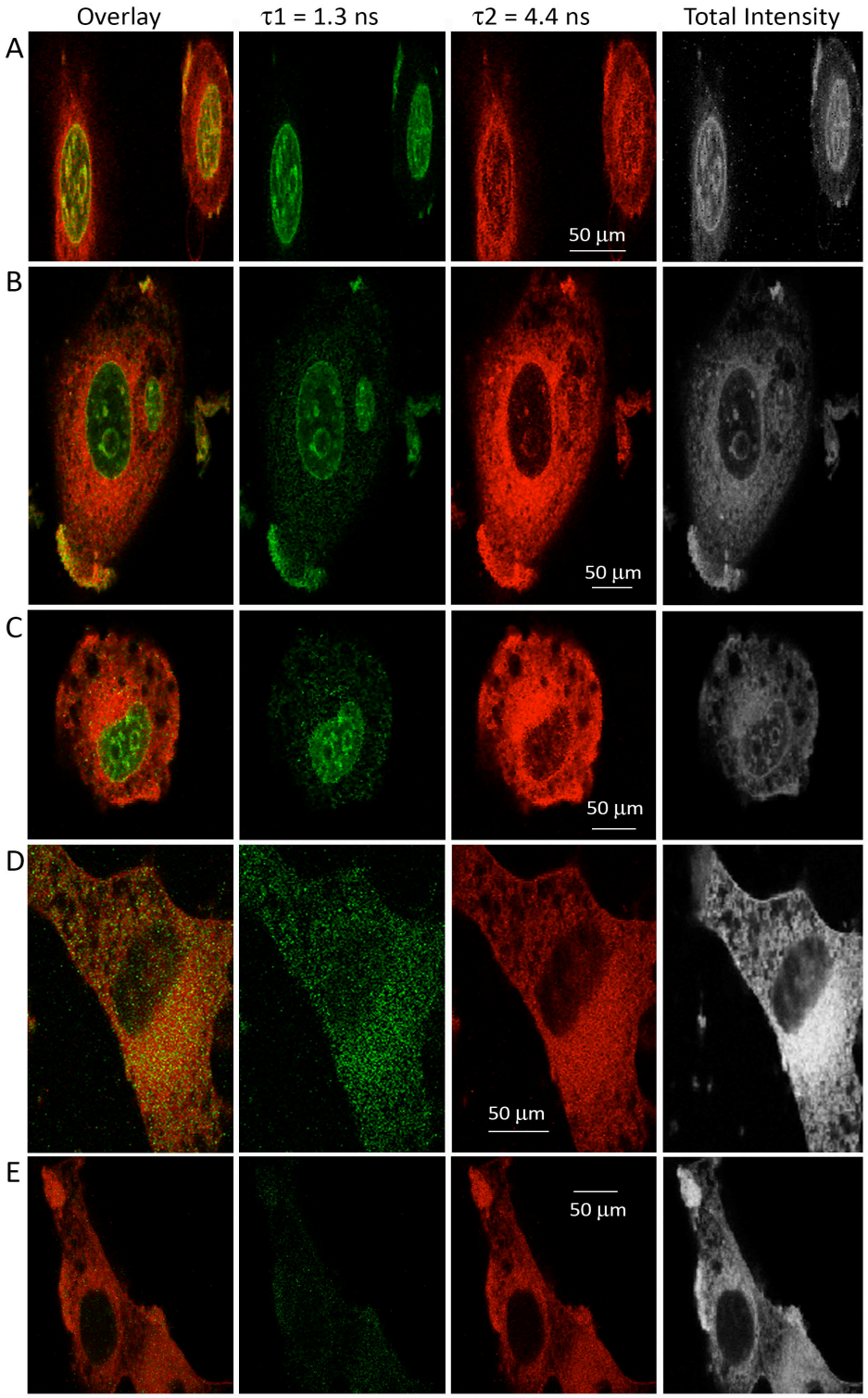

Figure 8. Best fits to fluorescence lifetime decays performed on a pixel-by-pixel basis in B16 cells incubated with Au-Dox. The errors on the lifetime fits are ± 0.1 ns. (A) 1 hour incubation. (B) 2 hour incubation. (C) 4 hours. (D) 12 hours, note the membrane and vesicular labelling in the intensity image that corresponds to the long-lifetime component. (E) 24 hours. Note the complete lack of nuclear signal.

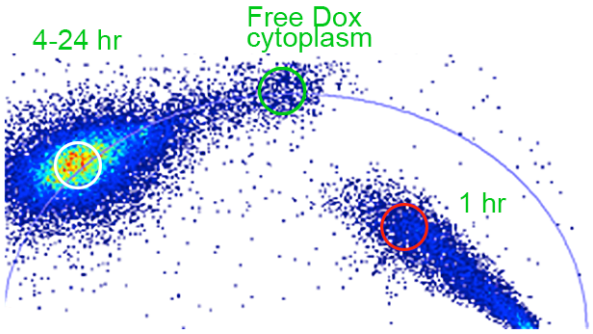

Figure 9. Phasor analysis of lifetimes from FLIM images. Single exponentials are located on the circle, whereas multiple exponentials are displaced from it.

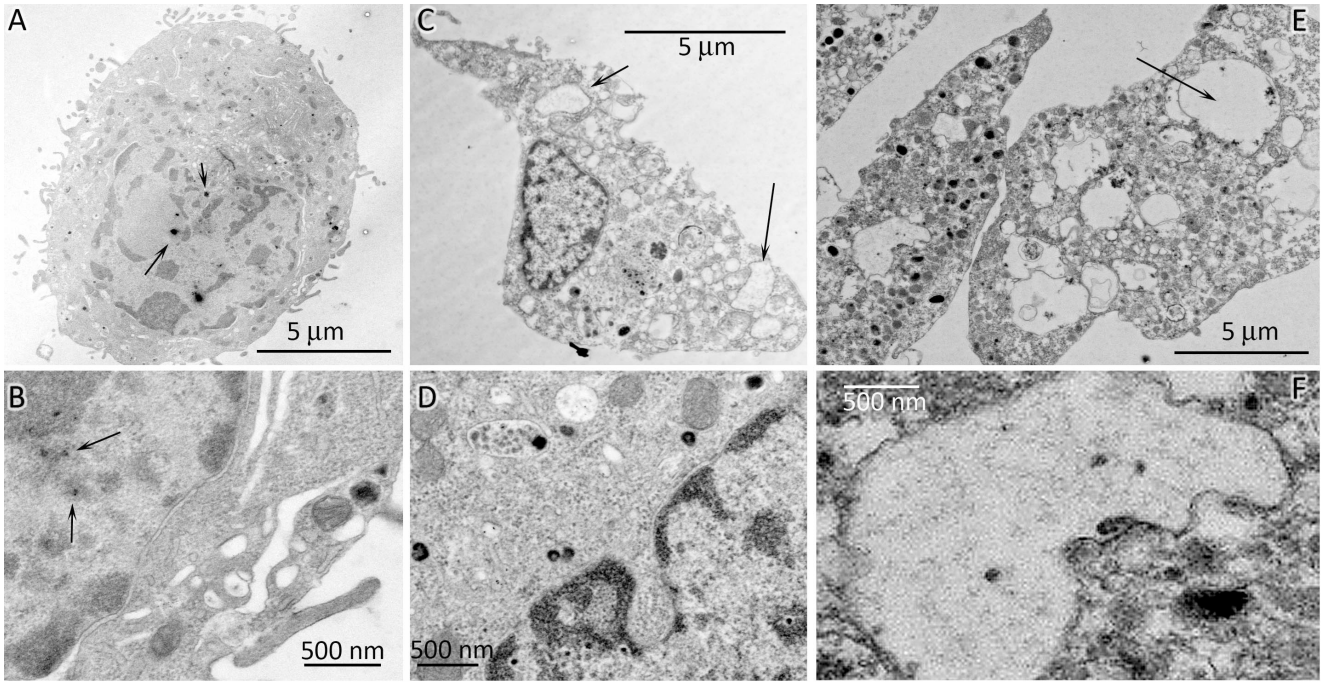

Figure 10. TEM images of Au-Dox labelled cells (for control images, see Supplementary Information **Fig. S4**). Gold appears as dark spots; larger areas do not necessarily indicate gold aggregation because of the staining process. (A) 1 hour incubation showing some Au inside the nucleus (arrows). (B) 1 hour incubation at higher magnification, showing intact nuclear membrane and very small Au clusters in the nucleus (arrows). (B) 6 hour incubation, showing a cell with a shrunken nucleus and Au surrounding the nuclear membrane as well as inside the nucleus and in the cytoplasm. Note the empty vacuoles indicating swollen mitochondria (arrows). (D) Higher magnification of 6 hour time point, showing Au build-up inside the nuclear membrane. (E) 24 hour time point, showing destruction of organelles and of the nucleus (arrow). (F) Higher magnification of 24 hour time point showing empty nuclear membrane.

TOC Graphic

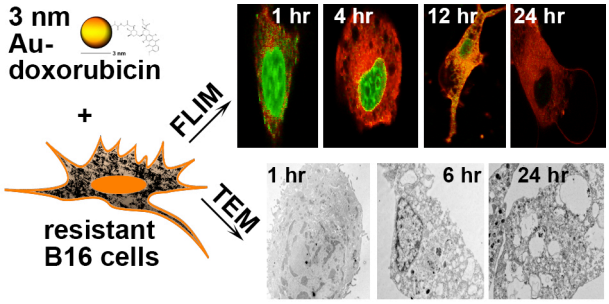

FLIM is used to observe uptake of stable gold-doxorubicin conjugates into cells and nuclei